

# The lives and deaths of star clusters near the Galactic center

Simon F. Portegies Zwart<sup>1</sup>\* Junichiro Makino<sup>2</sup> Stephen L. W. McMillan<sup>3</sup> Piet Hut<sup>4</sup>

\* SPZ is a Hubble Fellow

## ABSTRACT

We study the evolution and observability of young, compact star clusters near the Galactic center, such as the Arches and Quintuplet systems. The clusters are modeled by integrating the equations of motion of all stars while accounting for the internal evolution of the stars and binaries and the effect of the tidal field of the Galaxy. We find that clusters within 150 pc of the Galactic center dissolve within  $\sim 55$  Myr, but their projected densities drop below the background density in the direction of the Galactic center within only a few Myr, effectively making these clusters undetectable after that time. Detailed observations of the Arches cluster, when taken at face value, suggest that its mass function is unusually flat and that the cluster contains an overabundance of stars more massive than  $20 M_{\odot}$ . Our dynamical analysis, however, shows that the observed characteristics of the Arches cluster are consistent with a perfectly normal initial mass function. The observed anomalies are caused by a combination of observational selection effects and the dynamical evolution of the cluster. We calibrate the current parameters of the Arches cluster using a normal mass function and conclude that the cluster is more massive than  $40000 M_{\odot}$ , has a half mass radius of about 0.35 pc, and is located between 50 and 90 pc from the Galactic center.

*Subject headings:* binaries: close — stars: blue stragglers — stars: evolution — globular clusters: general — globular clusters: 30 Doradus, Arches, Quintuplet —

## 1. Introduction

A number of young, dense star clusters have been observed within the inner few hundred parsecs of the Galactic center. Best known are the Arches cluster (Object 17, Nagata et al. 1995) and the Quintuplet cluster (AFGL 2004, Nagata et al. 1990; Okuda et al. 1990). However, it is likely that others exist, as these clusters lie behind thick layers of obscuring material (Portegies Zwart et al. 2001a). Most are expected to be invisible at optical wavelengths, but should be readily detectable in the infrared (Vrba et al. 2000).

The Arches and the Quintuplet clusters are the Galactic counterparts of NGC 2070 (R 136), the central star cluster in the 30 Doradus region in the Large Magellanic Cloud (Massey & Hunter 1998). The structural parameters of these clusters—masses, radii, and density profiles—are quite similar, as are their ages. R 136, however, is located far from the perturbing influence of the Galaxy and the tidal effect of the

---

<sup>1</sup>Massachusetts Institute of Technology, Cambridge, MA 02139, USA

<sup>2</sup>Department of Astronomy, University of Tokyo, 7-3-1 Hongo, Bunkyo-ku, Tokyo 113-0033, Japan

<sup>3</sup>Department of Physics, Drexel University, Philadelphia, PA 19104, USA

<sup>4</sup>Institute for Advanced Study, Princeton, NJ 08540, USA

LMC is negligible. The Arches and the Quintuplet clusters, on the other hand, lie at a projected distance of  $\lesssim 50$  pc of the Galactic center, and their evolution is strongly affected by the Galactic tidal field.

A number of intriguing questions about these clusters make them worthy of detailed study: (1) how are these clusters related to globular star clusters, (2) how many of these clusters have yet to be discovered, (3) what is their contribution to the star formation rate in the Galaxy, and (4) are their mass functions intrinsically flat, as is suggested by observations? We address these questions using a fully self-consistent star-cluster model in which the dynamics of stars are followed by direct  $N$ -body integration, and the evolution of individual stars and binaries are followed using a stellar and binary evolution program.

The numerical methods are discussed in Sect. 2. Sect. 3 describes in more detail the initial conditions for our models. The results are presented in Sect. 4 and discussed in Sect. 5. We summarize and conclude in Sect. 6.

## 2. The model

The  $N$ -body portion of the simulations is carried out using the **kira** integrator operating within the “Starlab” software environment. Time integration of stellar orbits is accomplished using a fourth-order Hermite scheme (Makino & Aarseth 1992). **Kira** also incorporates block time steps (McMillan 1986; Makino 1991) special treatment of close two-body and multiple encounters of arbitrary complexity, and a robust treatment of stellar and binary evolution and stellar collisions. The special-purpose GRAPE-4 (Makino et al. 1997) system is used to accelerate the computation of gravitational forces between stars. The treatment of stellar mass loss is described by Portegies Zwart et al. (1998). A concise description of the Starlab environment is given by Portegies Zwart et al. (2001b); additional information is available at <http://www.manybody.org>.

Evolution of stars and binaries is handled using the prescription given by Portegies Zwart & Verbunt (1996, Sect. 2.1). However, some changes are made to the treatment of main-sequence mass loss in massive stars (see Portegies Zwart et al. 1999), and we incorporate a more extended prescription for stellar collisions, as described by Portegies Zwart, Hut & Verbunt (1997).

The system of units used internally in the  $N$ -body models is defined by  $M = G = -4E = 1$ , where  $E$  is the initial internal energy of the stellar system,  $M$  is the total mass in stars and  $G$  is the gravitational constant (Heggie & Mathieu 1986). For the runs considered here, the  $N$ -body and physical length scales are connected by the requirement that initially the star cluster is in virial equilibrium and exactly fills its zero-velocity surface in the Galactic tidal field (see Sect. 3.1 below). Once the cluster mass and distance to the Galactic center are known, the virial radius  $r_{\text{vir}}$  is determined, and the  $N$ -body time unit of the system may be conveniently expressed in physical units as

$$t_{\text{hm}} \simeq 42 \left( \frac{[M_{\odot}]}{M} \right)^{1/2} \left( \frac{r_{\text{vir}}}{[\text{pc}]} \right)^{3/2} [\text{Myr}]. \quad (1)$$

The half-mass relaxation time is calculated as (Spitzer 1987):

$$t_{\text{hrx}} = \left( \frac{r_{\text{hm}}^3}{GM} \right)^{1/2} \frac{N}{8 \log \Lambda}. \quad (2)$$

Here  $\Lambda \equiv \gamma N$  is the coulomb logarithm;  $\gamma$  is a scaling factor introduced to model the effects of the cut-off in

the long range Coulomb logarithm (see Giersz & Heggie 1996; 1994). For most density profiles the half-mass radius  $r_{\text{hm}}$  is slightly ( $\lesssim 25\%$ ) smaller than  $r_{\text{vir}}$ .

### 3. Selection of initial conditions

The two clusters on which we concentrate here, the Arches and the Quintuplet, lie in projection within  $\sim 50$  pc of the Galactic center. Table 1 lists some observed parameters of these clusters, along with some other clusters having comparable characteristics. All have masses of  $\sim 10^4 M_{\odot}$ , are very compact  $r_{\text{hm}} \lesssim 1$  pc, and are only a few million years old. However, of the systems listed, only the Arches and Quintuplet are significantly perturbed by external tidal fields.

Table 1: Observed parameters for some young, dense clusters. Columns give the cluster name, reference, age, mass, distance to the Galactic center (the cluster R 136 is located in the Large Magellanic Cloud), the tidal radius and the half-mass radius. The last two columns give the density within the half-mass radius and the half mass relaxation time.

Name	ref	Age [Myr]	M $[10^3 M_{\odot}]$	$r_{\text{GC}}$	$r_{\text{tide}}$ [pc]	$r_{\text{hm}}$	$\rho_{\text{hm}}$ $[10^5 M_{\odot}/\text{pc}^3]$	$t_{\text{hrx}}$ [Myr]
R 136	a	2–4	21–79	LMC	$\gtrsim 20$	$\sim 0.5$	0.4–1.5	70
Arches	b	1–2	12–50	30	1	0.2	3.6–15	12
Quintuplet	c	3–5	10–16	35	1	$\sim 0.5$	0.14–0.31	12
NGC 3603	d	2–3	3–13	few k	4–5	0.23	0.59–2.6	44
W43 (=G30.8-0.2)	e	$\lesssim 10$	?					
<i>nameless</i>	f	$\lesssim 10$	?	12–15k	$> 1$	0.2–0.4	0.45–4.5	

References: a) Brandl et al. (1996); Campbell et al. (1992); Massey & Hunter (1998). b) Figer et al. (1999); c) Glass, Catchpole & Whitelock (1987); Figer, McLean & Morris (1999). d) Brandl (1999) e) Blum, Damineli & Conti (1999) f) Vrba et al. (2000) \* Contains approximately 100 spectral type O and WN stars but further information is not available.

• Contains at least 13 early type O stars, the cluster does not have a name.

#### 3.1. The tidal field near the Galactic center

A star cluster embedded in the Galactic tidal field is not spherically symmetric. Rather, it is flattened and the stellar velocity distribution is anisotropic, particularly in the outer regions. The initial models which best describe such a cluster are the anisotropic density profiles described by Heggie & Ramamani (1995). As in the usual spherically symmetric King (1966) models, the density profile is described by the dimensionless parameter  $W_0$ . Higher values of  $W_0$  indicate a more centrally concentrated cluster (see the illustration in Fig. 1).

Following Heggie & Ramamani, we model the tidal potential  $\phi_T$  by the quadrupole formula

$$\phi_T(x, y, z) = -\frac{1}{2}(\alpha_1 x^2 + \alpha_3 z^2). \quad (3)$$

The cluster is taken to move on a circular orbit around the Galactic center. The  $x$ -axis in the rotating frame of reference centered on the cluster always points toward the Galactic center; the  $z$ -axis is perpendicular to the orbital plane. The quantities  $\alpha_1(> 0)$  and  $\alpha_3(< 0)$  are conveniently expressed in terms of the kinematic Oort constants  $A$  and  $B$  (Oort 1927) and the local Galactic density  $\rho_G$  as:

$$\begin{aligned}\alpha_1 &= -4A(A - B), \\ \alpha_3 &= 4\pi G \rho_G + 2(A^2 - B^2).\end{aligned}\quad (4)$$

Loosely speaking, we can think of  $\alpha_1$  as determining the overall strength of the tidal field, while the ratio  $\alpha_1/\alpha_3$  determines its geometry.

The Oort constants  $A$  and  $B$  are defined as

$$\begin{aligned}A &= \frac{1}{2} \left( \frac{v_c}{r} - \frac{dv_c}{dr} \right), \\ B &= -\frac{1}{2} \left( \frac{v_c}{r} + \frac{dv_c}{dr} \right),\end{aligned}\quad (5)$$

where  $v_c$  is the circular rotational velocity:

$$v_c = \sqrt{\frac{GM_{\text{Gal}}(r)}{r}}. \quad (6)$$

Taking the mass of the Galaxy within the cluster's orbit at distance  $r_{\text{GC}}$  ( $\lesssim 100$  pc) from the Galactic center to be (Mezger et al. 1999)

$$M_{\text{Gal}}(r_{\text{GC}}) = 4.25 \times 10^6 \left( \frac{r_{\text{GC}}}{[\text{pc}]} \right)^{1.2} M_{\odot}, \quad (7)$$

we find

$$\begin{aligned}v_c &= 136.8 \left( \frac{r}{[\text{pc}]} \right)^{0.1} \text{ km s}^{-1} \\ \frac{dv_c}{dr} &= 13.7 \left( \frac{r}{[\text{pc}]} \right)^{-0.9} \text{ km s}^{-1} \text{ pc}^{-1}.\end{aligned}\quad (8)$$

and hence

$$\begin{aligned}A &\simeq 61.5 r_{\text{GC}}^{-0.9} \text{ km s}^{-1} \text{ pc}^{-1} \\ B &\simeq -75.3 r_{\text{GC}}^{-0.9} \text{ km s}^{-1} \text{ pc}^{-1} \\ \rho_G &\simeq 4.06 \times 10^5 r_{\text{GC}}^{-1.8} M_{\odot} \text{ pc}^{-3}.\end{aligned}\quad (9)$$

Table 2 lists these parameters at selected Galactocentric distances.

The distance from the center of the star cluster (of mass  $M$ ) to the first Lagrange point (the Jacobi radius) is

$$r_{\text{L1}} \equiv \left( \frac{-M}{\alpha_1} \right)^{1/3} \quad (10)$$

Substitution of Eq. 7 into Eq. 10 yields

$$r_{\text{L1}} \simeq 4.90 \times 10^{-3} \left( \frac{M}{[M_{\odot}]} \right)^{1/3} \left( \frac{r_{\text{GC}}}{[\text{pc}]} \right)^{0.6} \text{ pc}. \quad (11)$$

Table 2: Parameters for the Galactic tidal field of the calculated star clusters at selected distances from the Galactic center. Each row gives the distance to the Galactic center, the local stellar density, and the Oort  $A$  and  $B$  constants. The first row gives that value for the local stellar density from Hill, Hiditch & Barnes (1985) and the Oort constants in the solar vicinity from Olling & Merrifield (1998).

$r_{\text{GC}}$ [pc]	$\rho_G(r)$ [ $M_\odot/\text{pc}^3$ ]	$v_c$ [ $\text{km s}^{-1}$ ]	$A$ [ $\text{km s}^{-1} \text{pc}^{-1}$ ]	$B$ [ $\text{km s}^{-1} \text{pc}^{-1}$ ]
Sun	0.11	$184 \pm 8$	$11.3 \pm 1.1 \times 10^{-3}$	$-13.9 \pm 0.9 \times 10^{-3}$
34	711	193	2.55	-3.12
90	123	212	1.06	-1.30
150	49	224	0.67	-0.82

### 3.2. Initial cluster structure

We adopt initial models comparable to those observed for the Arches and the Quintuplet clusters. By varying the density profile and the distance to the Galactic center we study how the cluster evolution depends on the initial conditions.

Our calculations start with 12k (12288) stars at zero age. We assign stellar masses  $m$  in the range  $0.1 M_\odot < m < 100 M_\odot$  from the mass function suggested for the Solar neighborhood by Scalo (1986). The median mass of this mass function is about  $0.3 M_\odot$ ; the mean mass is  $\langle m \rangle \simeq 0.6 M_\odot$ . For models with 12k stars this results in a total cluster mass of  $\sim 7500 M_\odot$ . We adopt a mass function which is applicable to the Solar neighborhood rather than the flatter mass spectrum suggested by observations (see below) in order to determine whether the flat mass spectrum can be attributed to cluster dynamical evolution. Initially all stars are single, although binaries do form via three-body encounters, in which one star carries away the excess energy and angular momentum necessary for two other stars to become bound.

We adopt three standard distances from the Galactic center: 34 pc, 90 pc and 150 pc. The shape of the zero-velocity surface in the tidal field of the Galaxy only depends on  $\alpha_3/\alpha_1$ , which is independent of  $r_{\text{GC}}$ . This, however, does not directly mean that the models can be scaled with respect to the distance to the Galactic center using the relaxation time alone, as the time scale for stellar evolution decreases when the cluster is located further from the Galactic center. This results in a more active mass loss by stellar evolution for clusters which are farther away from the Galactic center.

Initial density profiles and velocity dispersions are taken from Heggie & Ramamani (1995) models with  $W_0 = 1$ ,  $W_0 = 4$  and  $W_0 = 7$ , for a total of 9 models. At birth the clusters are in virial equilibrium and exactly fill their critical zero-velocity surfaces (“Roche lobes”) in the Galactic tidal field. Tab. 3 presents a summary of the adopted initial models. Figure 1 indicates the shape and structure of models with  $W_0=1$ , 4 and 7 at  $r_{\text{GC}} = 150$  pc; models closer to the Galactic center are identical in shape, but the scale is different. The zero-velocity surfaces of the various models are represented as ellipses.

We test the reproducibility of our calculations by performing several calculations per set of selected initial conditions. Each calculation was performed twice with a different random seed. In addition, we performed a set of calculations without stellar evolution for models with  $W_0 = 1$ , 4 and 7. These same initial realizations were rerun with stellar evolution switched on, for  $r_{\text{GC}} = 34$  pc, 90 pc and 150 pc. The total number of calculations was 30.

Table 3: Overview of initial conditions for the simulations performed. Each row lists the model name, the distance to the Galactic center, the initial King parameter  $W_0$ , the initial relaxation time (see Eq. 2 and see paper IV for the version in more usual astronomical units) and half-mass crossing time, and the initial core radius, virial radius, and tidal radius. The final three columns give the number of stellar collisions observed in each calculation, the time of core collapse and the time at which the cluster mass dropped below 5% of the initial mass (about  $375 M_\odot$ ).

Model	$r_{GC}$	$W_0$	$t_{trx}$	$t_{hrx}$	$t_{hm}$	$r_{core}$	$r_{vir}$	$r_{tide}$	$n_{coll}$	$t_{cc}$	$t_{end}$
	[pc]		— [Myr]	— [Myr]	— [Kyr]	— [pc]	— [pc]	— [pc]			[Myr]
R34W1	34	1	53	5.5	43	0.12	0.20	0.76	5	1.9	7.4
R34W4	34	4	53	3.2	27	0.05	0.14	0.76	8	1.2	12.7
R34W7	34	7	53	0.36	9	0.018	0.077	0.80	24	0.4	12.0
R90W1	90	1	134	14.6	105	0.19	0.36	1.4	7	1.9	25.6
R90W4	90	4	134	8.1	68	0.09	0.26	1.4	15	1.2	32.6
R90W7	90	7	134	1.0	25	0.032	0.14	1.4	14	1.4	32.4
R150W1	150	1	218	23.6	169	0.30	0.50	1.9	5	2.0	45.8
R150W4	150	4	218	13	110	0.14	0.36	1.9	8	2.0	53.4
R150W7	150	7	218	4.5	40	0.044	0.19	2.0	14	0.4	55.0

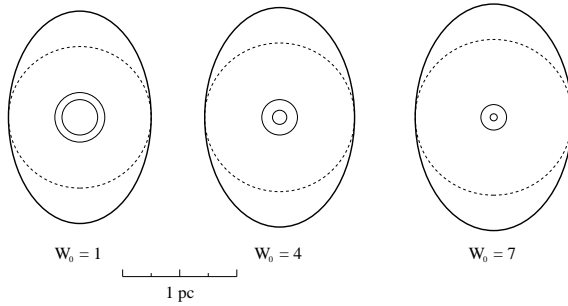


Fig. 1.— Illustration of the structure of star clusters with  $W_0=1$  (left),  $W_0=4$  (middle) and  $W_0=7$  (right). The outer ellipse represents the zero velocity surface of the cluster in the Galactic field. The two inner circles represent the half-mass and core radii. The dashed circle shows the 'tidal radius' that would be obtained if the initial model were described by King's spherically symmetric density profile. The Galactic center is to the top of the figure, at a distance of 150 pc. The length scale is indicated by the horizontal bar.

Stars are removed from the  $N$ -body system when their distance from the center of the cluster exceeds  $3r_{\text{L1}}$ . In the  $N$ -body calculations it is not always trivial to determine the moment the cluster dissolves, as a few stars may remain bound for an extended period of time (Portegies Zwart et al 1998). In our models we identify the cluster’s disruption as the moment when no stars lie within the zero velocity surface. Typically, a few hundred stars remain in the  $N$ -body system (within  $3r_{\text{L1}}$ ) at this time.

#### 4. Results

We first discuss the global parameters of all models. Later we will concentrate on a few representative models.

Figure 2(a) shows the mass evolution of the models listed in Table 3. Not surprisingly, clusters located at larger distances from the Galactic center tend to live longer than those closer to the Galactic center.

Figure 2(b) gives the mass evolution of several of our models with  $W_0 = 4$  at various distances from the Galactic center and compares the results with a model in which stellar evolution was not taken into account and in which stars were not allowed to collide. All the calculations presented in this figure were started with identical initial conditions. The only difference between the various runs is the distance from the Galactic center (varying from 34 to 150 pc) and whether stellar evolution is included in the calculation. In this figure, time is scaled with respect to each model’s initial relaxation time, i.e.:

$$t_{\text{rlx}} \propto N/8 \log(0.4N). \quad (12)$$

The various lines in Figure 2 do not overlap perfectly, mainly due to stochastic differences in the moments when exactly binaries are formed, etc. The small deviations from the model in which stellar evolution was not taken into account indicate that stellar evolution in these models is unimportant. If stellar evolution were important, clusters at greater distances from the Galactic center would dissolve more rapidly. However, we see the opposite trend: clusters farther from the Galactic center tend to dissolve slightly more slowly; the model without stellar evolution dissolves fastest. We have no ready explanation for this trend, but observe similar trends in our models with  $W_0 = 1$  and  $W_0 = 7$ . Note that this trend cannot be attributed to collisions, as they tend to heat the cluster, so clusters with higher collision rates (closer to the Galactic center) would dissolve more rapidly. This trend may be explainable in terms of the complex interplay between stellar evolution, binary formation and stellar collisions, but this possibility requires more detailed study, and is beyond the scope of this paper.

Figure 3 shows the time variation of the relaxation time for the models at 34 pc and 90 pc from the Galactic center. Note that the relaxation time measured some time after zero age contains little information about the clusters’ initial conditions. The behavior of the half-mass relaxation time is qualitatively similar to that found in less compact clusters at greater distances (6–12 kpc) from the Galactic center (Portegies Zwart et al. 2001b)—it first rises by a factor of a few as the cluster expands, then slowly decreases as the cluster loses mass.

Figure 4(a) shows the evolution of the mean densities within the half mass radius in models R150W1, R90W4 and R34W7. The initial half mass densities for these models were very different, ranging about three orders of magnitude. At later times the differences in the half mass densities become much smaller; after five million years the difference has decreased to about a factor 5.

As in Fig 2, Figure 4(b) also shows the densities of the models as functions of time scaled to the initial

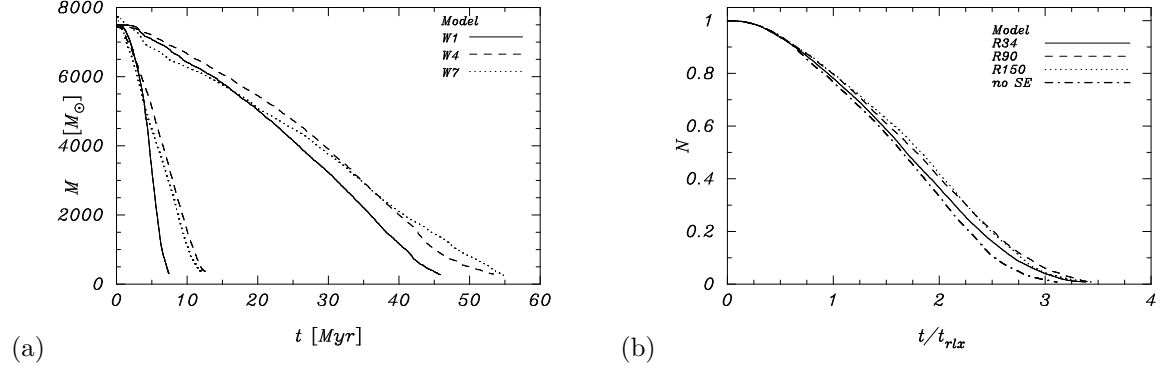


Fig. 2.— (a) Evolution of total cluster mass for models with  $W_0=1$  (solid lines),  $W_0=4$  (dashed lines) and  $W_0=7$  (dots) at distances of 34 pc (left lines) and 150 pc (right) from the Galactic center. (b) The evolution of the number of stars (renormalized to the initial total of 12k) for the models with  $W_0=4$  as a function of time in units of the initial relaxation time (see Eq. 12) for  $r_{\text{GC}} = 34$  (solid),  $r_{\text{GC}} = 90$  (dashes) and  $r_{\text{GC}} = 150$  (dots). The dash-dotted line gives the evolution of the number of stars for the model without stellar evolution. These models were all calculated using the same realization of the initial conditions.

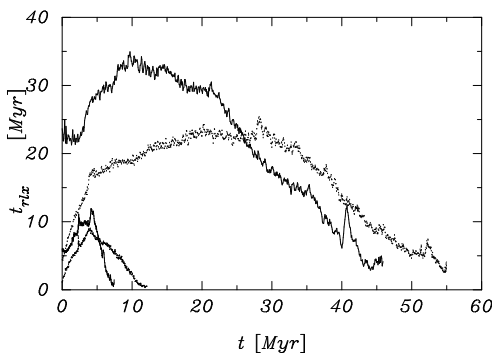


Fig. 3.— Evolution of the half-mass relaxation time for clusters lying 34 pc and 150 pc from the Galactic center, and with  $W_0=1$  (solids) and  $W_0=7$  (dotted lines). The models with  $W_0=4$  and those at  $R_{\text{rg}} = 90$  pc are not given.

relaxation time. The trend, visible in Fig 2, is somewhat obscured due to random fluctuations in the density. These fluctuations, however, are consistent with expectations (see Portegies Zwart et al 2001a and Baumgardt 2001).

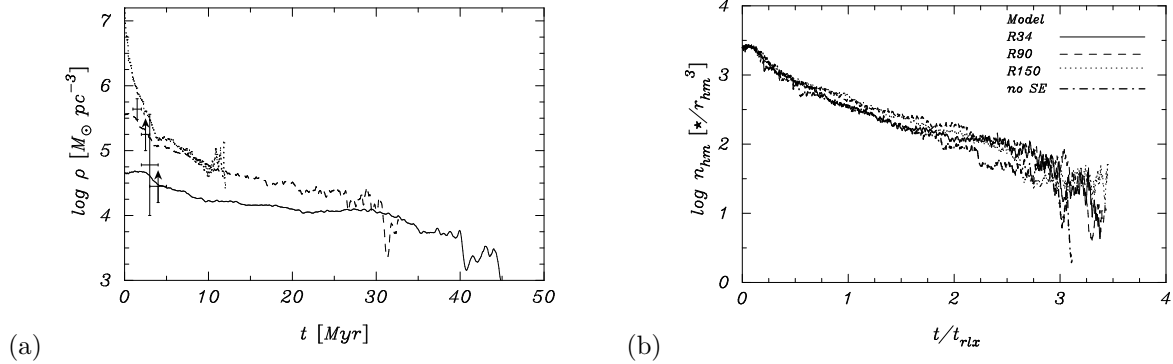


Fig. 4.— Evolution of the half mass density for clusters. (a) panel in astronomical units ( $M_\odot \text{ pc}^{-3}$  for the models R150W1 (solid), R90W4 (dashes) and R34W7 (dots). Error bars give the values for age and core density listed in Table 1. (b) the density evolution of the models with  $W_0=4$  but now in  $N$ -body units [see also panel (b) in Fig. 2].

Figure 5 shows the evolution of the core radius, selected Lagrangian radii, and the Jacobi radius  $r_{L1}$ , for model R90W4. Core collapse occurs within  $\sim 1.2$  Myr followed by a gradual overall expansion of the cluster. Similar behavior is evident in the isolated clusters considered by Portegies Zwart et al. (1999). The post-collapse expansion stops after a few million years, by which time the relaxation time has reached its maximum value (see Fig. 3). Subsequently, the Lagrangian radii decrease as the Jacobi radius shrinks and the cluster dissolves.

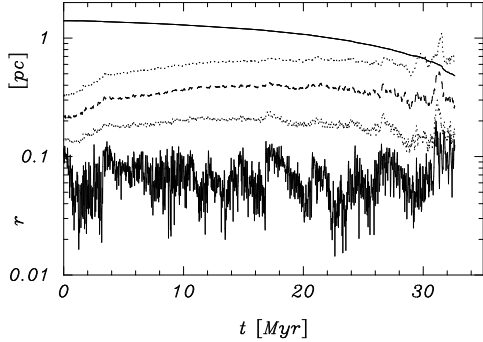


Fig. 5.— Evolution of the core radius (lower solid) and the 25%, 50% and 75% Lagrangian radii (dots, dashes and upper dotted lines, respectively) for model R90W4. The top line shows the instantaneous Jacobi radius of the cluster.

Figure 6 shows the evolution of the fraction of stars having masses greater than  $1 M_\odot$ , within the 5%

Lagrangian radius and near the 50% and 75% Lagrangian radii of model R90W4. Mass segregation causes the central mass function to flatten rapidly, but it takes considerably longer before the outer region of the cluster is significantly affected. After  $\sim 4$  million years, the mass function within the inner 5% Lagrangian radius contains about 4 times as many stars with masses exceeding  $1 M_\odot$  (relative to the local number density) than does the rest of the cluster. The mass function near the half-mass radius remains comparable to that of the cluster as a whole (see also Vesperini & Heggie 1997). The outer 75% of the cluster becomes slightly depleted of high mass stars. Within one initial half-mass relaxation time, the fraction of stars with  $m > 1 M_\odot$  in this region falls with about a factor of 3. At later times, the fraction of high mass stars throughout the cluster increases due to the preferential escape of low-mass stars. At disruption, the cluster is rich in high-mass stars, while low-mass stars are depleted. Takahashi & Portegies Zwart (2000) concluded that the observed flat mass function in the globular cluster NGC 6712 indicates that this cluster is close to dissolution.

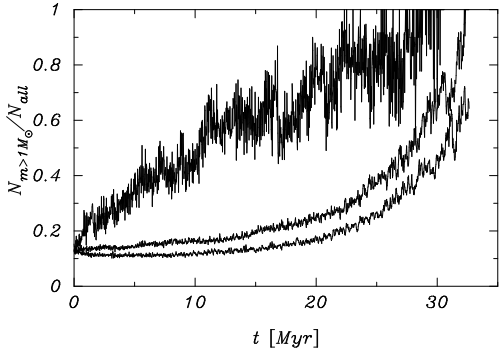


Fig. 6.— Fraction of stars having masses  $> 1 M_\odot$  within the 0–5% (upper line), 10–50% (middle line), and 50–90% (lower line) Lagrangian radii, for model R90W4.

Figures 7 shows the evolution of the binding energy ( $-E_{\text{tot}}$ , in scaled  $N$ -body units) for models R90W4 and R90W7, which are selected for their similar lifetimes. (Some deviations between the solid and the dotted lines are a result of our definition of a binary. Here we consider a binary to be a pair of bound stars for which the internal forces are a hundred times higher than those of the nearest neighbor.) Initially, each cluster has  $E_{\text{tot}} = -0.25$  (see Sect. 2), but due to escapers, binary activity, stellar mass loss, mergers, supernovae, etc., the total energy changes. A cluster ceases to exist when its binding energy becomes positive. The two clusters exhibit quite similar global evolution. Model R90W4 shows an initial “plateau” of a few Myr during which the mass segregation occurs, driving the cluster to its phase of core collapse. For model R90W7 this phase is hardly noticeable as the cluster almost directly goes to core collapse.

During the first deep core collapse the binding energy fluctuates rapidly because binaries frequently harden and single stars are ejected following three-body encounters. The first collisions happen during this phase (see • in fig. 7) and in both models mass transfer occurs in a dynamically formed binary, giving rise to an excursion in the binding energy (see the dotted line in Fig. 7). Core collapse is followed by the ejection of a hard binary (arrows in Fig. 7).

After the first collapse of the core the binding energy of both cluster decreases steadily with some strong fluctuations caused by close two and three body encounter (triangles in fig. 7), high-velocity escapers

(arrows), stellar collisions ( $\bullet$ ), mass transfer in close binaries and supernovae ( $\star$ ).

Model R90W7 experiences much more binary activity than model R90W4. This can be seen from the many excursions of the dotted line in Fig. 7. Such excursions are the result of binary activity, such as mass transfer. A stable phase of mass transfer generally results in an excursion in the binding energy of the binary. Such binaries will first become very hard as the orbital period decreases and soften when the mass of the donor drops below that of the accreting star. One example of this is very clearly visible in panel (b) of Fig. 7, where around  $t = 11$  Myr, the dotted line starts an excursion. The phase of mass transfer stops after about 3 Myr, indicating that it is a case A (Kippenhahn & Weigert 1967), i.e.: stable on a nuclear time scale (see also Portegies Zwart et al. 2001b). This episode stops when the donor leaves the main sequence, becomes an envelope-depleted helium burning star and finally explodes in a supernova (filled star). The mass loss in the supernova, forming a black hole, causes the the binary to be ejected from the cluster (up pointed arrow).

The spikes to lower binding energy in both model R90W4 and R90W7 are the result of stars which receive a high velocity upon a strong encounter. Such a high energy encounter may decrease the binding energy of the entire cluster for as long as the star is considered a cluster member (within  $3r_{L1}$  from the cluster center). Model R90W7 produces many more high velocity escapers than model R90W4, which also indicates the greater dynamical activity within the more compact cluster.

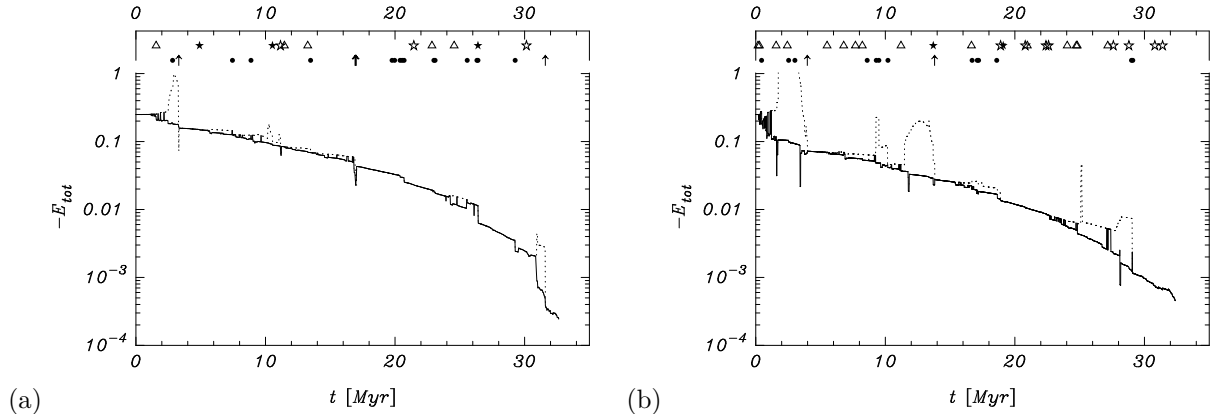


Fig. 7.— Evolution of the binding energy for models R90W4 (a) and R90W7 (b). Solid lines include the binding energies of all stars (only the center of mass energy of binaries and higher order systems are included) the dotted lines include the binding energies of the binaries. Initially  $E_{\text{tot}} = -0.25$  (see Sect. 2). The two lines with symbols in the horizontal bar above the figure indicate important happenings in the cluster lifetime. Triangles indicate the moment at which a binary or triple is formed by a three- (or more) body interaction, the filled and open asterisks indicate the formation of a black hole and neutron star, respectively. The filled circles indicate the moment a collision occurs and arrows pointing upward indicate the moment then a hard binary is ejected from the cluster. All these events are reflected in the evolution of the binding energy.

## 5. Discussion

The Arches and the Quintuplet are among the youngest star clusters known in the Galaxy. They are not as rich as small globular clusters, but considerably more compact. Their central densities are

comparable to those of the densest—post collapse—globulars, but their life expectancies are only a few tens of millions of years. These clusters are destroyed by tidal forces, accelerated by impulsive mass loss from supernovae (after  $\sim 3$  Myr) and strong binary activity. The discussion that follows focuses on the comparison with the well observed Arches cluster. First we compare the observed mass function with the results from our models followed by the observed density profile. We then discuss the consequences with respect to the inferred distance of the Arches and Quintuplet clusters from the Galactic center and the number of such clusters which may still be hidden near the Galactic center.

### 5.1. Comparison with observations

Figer et al. (1999) studied the mass function of the Arches cluster in two projected annuli, the inner one spanning 2.5 to 4.5 arc seconds from the cluster center (0.098 to 0.18 pc, assuming a distance of 8 kpc), and the outer one extending from 4.5 to 7.5 arc seconds (0.18 to 0.29 pc). They found that the cluster mass function is much flatter than the Salpeter distribution (a power law with exponent  $x = -2.35$ ), and that the mass function in the inner annulus is even flatter ( $x = +1$  to  $-1.5$ ) than that in the outer parts ( $x = -1.5$  to  $-2.0$ ). In the inner annulus they claim to be complete down to  $20 M_{\odot}$  and down to  $10 M_{\odot}$  in the outer annulus. The total number of stars in the inner annulus is 50 down to  $20 M_{\odot}$  resulting in a total mass of  $2173 M_{\odot}$ . The total number of stars in the outer annulus is 122 down to a mass of  $10 M_{\odot}$  resulting in a total mass of  $3164 M_{\odot}$ . The ratio of the mean mass in the outer annulus to that in the inner annulus is then  $f_{o/i} \equiv \langle m \rangle_{\text{out}} / \langle m \rangle_{\text{in}} \simeq 25.9 M_{\odot} / 43.5 M_{\odot} \sim 0.597$ .

This mean mass ratio  $f_{o/i}$  is a characteristic of the cluster. Its value is a complicated function of time and position in the cluster, and also of the initial mass function. For a Scalo (1986) mass function at zero age and in a system with a homogeneous density the value of this fraction is  $f_{o/i} = 0.501^5$ . As more massive stars sink to the cluster center due to mass segregation the value of  $f_{o/i}$  changes with time. The value of  $f_{o/i}$  also changes due to the variation of the density profile in the cluster and therefore is also a function of the distance from the cluster center where  $f_{o/i}$  is measured. We will compute  $f_{o/i}$  at various distances from the center of our model clusters with  $W_0 = 4$  and at various moments in time.

We selected a total of 6 sets of inner and outer annuli starting close to the cluster center and moving progressively outwards. For the innermost annulus we took  $r_{\text{in}} = 0.003125$ ,  $r_{\text{mid}} = 0.05625$  and  $r_{\text{out}} = 0.09375$  (in units of the initial virial radius) and we increased the radii by factors of two for subsequent annuli out to  $r_{\text{in}} = 1.0$ ,  $r_{\text{mid}} = 1.8$  and  $r_{\text{out}} = 3.0$ . For each of our  $N$ -body calculations we computed  $f_{o/i}$  for all combinations of 6 inner and outer annuli. To improve statistics we then combined the values for the inner two (solid line), the middle two (dashes) and the outer two (dotted line) annuli.

Figure 8 plots these values of  $f_{o/i}$  as a functions of time for our model calculations with  $W_0 = 4$ , compares them with the observed mass function. We combined all models with  $W_0 = 4$  to improve the statistics at the top end of the mass function. We computed a total of 14 models with these parameters, of which 8 were run for only 0.91 initial relaxation times and 6 continued until they dissolved (more than  $3 t_{\text{hrx}}$ ). The various models were scaled to the initial relaxation time before being superposed, as explained in Sect. 4. At later times ( $t \gtrsim t_{\text{hrx}}$ ) some effect from stellar evolution may be influencing this scaling, but since we are mostly concerned in the earlier times this does not affect our conclusions.

---

<sup>5</sup>The initial value of  $f_{o/i} < 1$  because of the different lower cut offs in the nominator and the denominator.

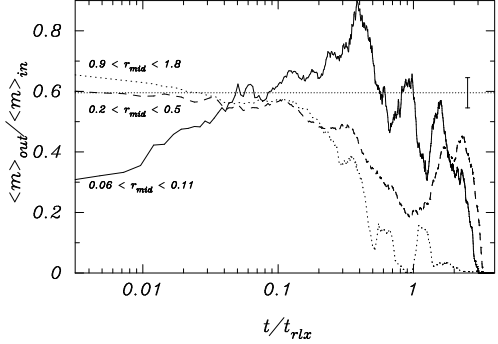


Fig. 8.— The values for  $f_{o/i}$  (the mass ratio of the mean mass in the outer annulus divided by the mean mass in the inner annulus) as a function of the time in units of the initial relaxation time. Each of the various lines combines the results for two of the measured values for  $f_{o/i}$ . The solid line gives the sum of inner two values (with  $r_{\text{mid}} = 0.06$  and  $0.11$ ), dashed line for the intermediate range ( $r_{\text{mid}} = 0.2$  and  $0.5$ ) and the dotted line gives the value of  $f_{o/i}$  for the outer annuli ( $r_{\text{mid}} = 0.9$  and  $1.8$ ). The horizontal dotted line gives the measured value of  $f_{o/i}$  as measured by Figer et al. (1999) with the Poissonian error bar (at right).

The observed value of  $f_{o/i}$  (error bar) may be moved along the horizontal dotted line until it fits with any of the other curves, which represent the model calculations. A matching result indicates that the observed mass function at these annuli agrees with a cluster at the appropriate age in units of its initial relaxation time. We illustrate this with a few examples.

At later times ( $t \gtrsim 0.1 t_{\text{hrx}}$ ) the observations fit quite nicely with the solid line in Fig. 8, representing the innermost annuli. Initially, high-mass stars are under abundant in the inner part of the cluster, and only at later times does mass segregation cause them to sink to center of the potential well of the system, explaining the initial rise in  $f_{o/i}$  for the innermost annuli. If indeed the observed value of  $f_{o/i}$  coincides with the model calculations at the innermost part of the cluster, the observed cluster must be older than about  $t \gtrsim 0.1 t_{\text{hrx}}$ . At an observed age of the Arches cluster of 1–2 Myr the initial relaxation time must then have been  $t_{\text{hrx}} \lesssim 20$  Myr. Using the intermediate annulus of  $r_{\text{mid}} = 0.18$  pc to set the size scale of the models, the half-mass radius of the Arches cluster is then  $r_{\text{hm}} \gtrsim 1.6$ – $3.0$  pc. A cluster with a half-mass radius of  $r_{\text{hm}} \gtrsim 1.6$  pc and a relaxation time  $t_{\text{hrx}} \lesssim 20$  Myr contains less than a hundred stars. Since the number of stars observed easily exceeds this number we can firmly reject this solution: the observed radius of  $r_{\text{mid}} = 0.18$  pc then corresponds to  $\lesssim 2 r_{\text{vir}}$ .

Alternatively, we observe the cluster when it is younger in terms of its relaxation time. In the very early evolution of the cluster  $t \lesssim 0.05 t_{\text{hrx}}$  the observations are quite consistent with  $0.2 \lesssim r_{\text{mid}} \lesssim 1.8$  (the dashed as well as with the dotted line in fig. 8), but is inconsistent with  $r_{\text{mid}} \lesssim 0.11$ . The intermediate radius in the observations corresponds to  $r = 4.5''$  (or about 0.18 pc at a distance of 8 Kpc). With these values the cluster would be described accurately by  $r_{\text{vir}} = 0.1$  to  $0.9$  pc at an age  $\lesssim 0.05 t_{\text{hrx}}$ . With an age of the Arches cluster of 1–2 Myr (see Tab. 1) the initial relaxation time of the cluster must be smaller than 20–40 Myr. With a half-mass radius  $r_{\text{vir}} \lesssim 0.9$  (corresponding to  $r_{\text{hm}} \simeq 0.75$  pc), the cluster then has a mass of about  $4000 M_{\odot}$  in order to produce a half-mass relaxation time of  $t_{\text{hrx}} \lesssim 40$  Myr. If  $r_{\text{vir}} = 0.1$  pc, the total mass is  $2.4 \times 10^6 M_{\odot}$  and the relaxation time is 20 Myr.

Taking the observed half mass radius of  $r_{\text{hm}} \sim 0.2$  pc and correcting it for the effects of mass segregation and expansion during its early dynamical evolution to  $r_{\text{hm}} \sim 0.35$  pc, a relaxation time of 30 Myr implies a cluster of about 64k stars and a total mass of about  $40\,000 M_{\odot}$ . These numbers would also agree with the observed number of massive stars (50 stars with  $m > 10 M_{\odot}$  in the inner annulus) if a normal Scalo (1986) mass function would be adopted. We thus see no reason to invoke a flatter than usual mass function to explain the observations. This is consistent with the suggestion of Serabyn, Shupe & Figer (1998) that the Arches contains  $\sim 10^5$  stars, far more than the 12k adopted in our models or as was suggested by Figer et al. (1999).

Adopting that the density profile of the cluster is consistent with a King model with  $W_0 = 4$  to 6 and adopting  $r_{\text{hm}} = 0.35$ , we derive a Jacobi radius of 1.6 pc to 2.5 pc, respectively. The consequence would be that the distance of Arches cluster to the Galactic center is between 43 pc and 91 pc, for a model with  $W_0=4$  or  $W_0=6$ , respectively. We conclude that the Arches cluster is likely to be at a distance from the Galactic center somewhat, but not much, greater than its projected distance. Table 4 reviews our conclusions about the Arches cluster.

Table 4: Proposed parameters for the Arches cluster resulting from our best values from our model calculations. Assuming a normal mass function comparable to that of the Solar neighborhood. These numbers are derived and discussed in the sections 5.1, 5.2 and 5.3.

parameter	value
$M$	$\sim 40000 M_{\odot}$
$N$	$\sim 65000$ stars
$r_{\text{GC}}$	43 — 91 pc
$t_{\text{hrx}}$	20 — 40 Myr
age	$0.05 \pm 0.02 t_{\text{hrx}}$
$r_{\text{hm}}$	$0.35 \pm 0.05$ pc
$r_{\text{vir}}$	$0.42 \pm 0.05$ pc
$W_0$	4 — 6
$r_{\text{tide}}$	1.6 — 2.5 pc

## 5.2. The density profile

Figure 9 shows the projected density profile of our model clusters with  $W_0=4$  for stars having masses  $m \gtrsim 20 M_{\odot}$  at various instants. The data are presented in virial units (horizontal axis in units of  $r_{\text{vir}}$ , and the vertical axis in units of stars per  $r_{\text{vir}}^{-2}$ ). The various curves (and symbols) represent the density distribution of the model clusters at zero age (solid line), at  $t = 0.05$  initial relaxation times (dashes), and at  $t = 0.5t_{\text{hrx}}$  (dotted line). Mass segregation causes the density profile of the older clusters to steepen with time, tidal stripping causes the global density to decrease.

The open squares in Fig. 9 present the observed density distribution for the Arches cluster (Figer et al. 1999). These data are given in arc seconds (or parsec when scaled to the appropriate distance). We plot them in the same figure assuming that the observed medium radius of 0.18 pc (4.5 arc-seconds) corresponds to  $0.18r_{\text{vir}}$ , i.e.: that the virial radius of the Arches cluster is 1 pc. This may be a bit of an overestimate, as is discussed in the previous section. There is some freedom in shifting the observed points along the arrow,

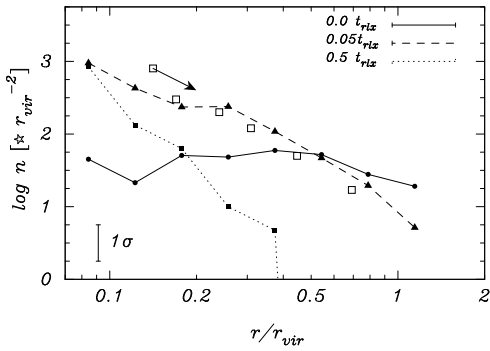


Fig. 9.— Projected density profile of the Arches cluster for stars with  $m > 20 M_{\odot}$  from the observations of Figer et al. (1999; data from Kim et al. 2000—open squares). These data were scaled to a virial radius of 1 pc. The arrow starting from the upper left most square indicates the direction in which to shift these symbols when the size scaling (in arc-seconds) is increased by  $1\sigma$ . They adopted the inner annulus between  $2.5 < r < 4.5$  arc-seconds ( $0.098 < r < 0.18$  pc) and an outer annulus between  $2.5 < r < 4.5$  arc-seconds ( $0.18 < r < 0.29$  pc). The various other lines and symbols give the results of our  $N$ -body calculations with  $W_0 = 4$ . The various lines represent the density profile at the moment indicated (top right corner). These moments are presented in units of the initial relaxation time of our models, ranging from zero age (solid line) to  $0.5 t_{\text{hrx}}$ . The densities for our model calculations were increased with a factor 64/12 to account for the larger number of stars expected in these clusters. In the lower left corner is a  $1\sigma$  Poissonian error bar for reference.

which then changes the scaling for the cluster.

The observed points fit best with the dashed line and are not consistent with the solid (zero age) or the dotted ( $t = 0.5t_{\text{hrx}}$ ) lines. The projected density profile of the observed Arches cluster thus suggests an age of about  $t \simeq 0.05 t_{\text{hrx}}$ , in agreement with our findings in section 5.1.

### 5.3. Distances to the Galactic center

The Arches cluster is located at a projected distance of  $\sim 30$  pc from the Galactic center, the Quintuplet at  $\sim 35$  pc. These measurements provide lower limits to the true distances of these clusters from the center.

The mean density within the Jacobi radius of a tidally limited cluster is proportional to the local stellar density. (This is not a matter of definition—it happens to be true for point-mass fields if you average the point mass over  $r_{\text{GC}}$ , and for the power-law density profiles we consider here, since the tidal field  $\sim M/R^3 \sim M_G/r_{\text{GC}}^3 \sim r_{\text{GC}}^{-2} dM_G/dr_{\text{GC}} = \rho_g$ , but it is not in general the case.) Thus, a cluster closer to the Galactic center is more compact, has a shorter relaxation time, and therefore evolves more rapidly than a similar cluster at a greater distance.

Most of our 34 pc models have densities higher than any of the observed clusters listed in Tab. 1 (see Fig. 4). Only the model with an extremely shallow initial density profile (R34W1) has density comparable to the observed systems. Clusters at greater distances from the Galactic center (but with the same projected distance) have lower densities. Since the densities of the 34 pc models are too high by at least a factor of two, this suggests that the real clusters are somewhat farther out, at  $r_{\text{GC}} \gtrsim 50$  pc; a factor of 2 in density corresponds to a factor of  $2^{1/3}$  in radius, so the true Galactocentric distance should exceed 43 pc.

Figure 10 plots the evolution of the mean surface density within the projected half-mass radius for models R34W7 (dots), R90W4 (dashes) and R150W1 (solid), which are the most extreme models. We view the clusters along the  $x$ -axis, so we look through the second and first Lagrangian points toward the Galactic center, giving the highest possible cluster density and hence an overestimate of the true density contrast (see Fig. 1). The two error bars give the projected half-mass densities for the Arches (left), and the Quintuplet (right) clusters. The horizontal dotted line gives the background surface density (from Eq. 9) at a projected distance of 34 pc from the Galactic center.

The surface density at projected distance  $d$  from the Galactic center can be calculated by integrating the local stellar density  $\rho_G$  (Eq. 9) along the line of sight to the cluster:

$$\Sigma(d) = 4.06 \times 10^5 \int (d^2 + z^2)^{-0.9} dz \text{ M}_\odot \text{ pc}^{-2}. \quad (13)$$

Integrating Eq 13 from -100 to 100 pc (the range of validity of the Mezgers' equation) gives the projected surface densities towards the Arches (at  $d = 30$  pc) and Quintuplet cluster (at  $d = 35$  pc). We integrate Eq. 13 numerically. Figure 11 illustrates this. An extra correction for stars between 100 pc from the Galactic center and Earth adds little ( $\lesssim 10\%$ ) to the total (Bahcall & Soneira 1980). The projected densities of the observed clusters are about an order of magnitude higher than the background. Clusters with lower background densities may well remain unnoticed among the background stars, as observers will likely have difficulty distinguishing them from the background. Note, however, that the background stellar population is probably older than the studied star clusters and may therefore have a smaller mass-to-light ratio, making the clusters stand out somewhat better against the background.

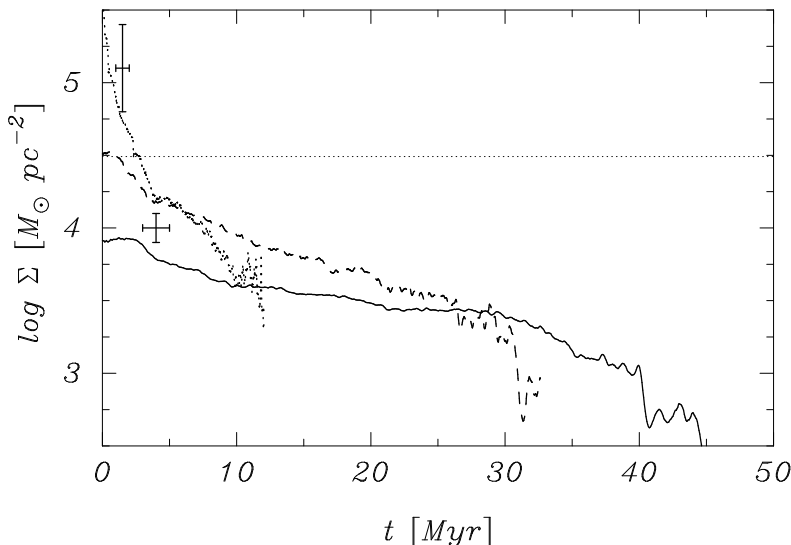


Fig. 10.— Evolution of the projected density within the half-mass radius for models R34W7 (dots), R90W4 (dashes), and R150W1 (solid). The dotted horizontal line gives the surface density at a projected distance of 34 pc from the Galactic center. The selected cases are quite extreme; R34W7 being the most concentrated model and R150W1 the least concentrated. The two error bars (to the left) indicate the location of the Arches (left) and the Quintuplet (right) clusters.

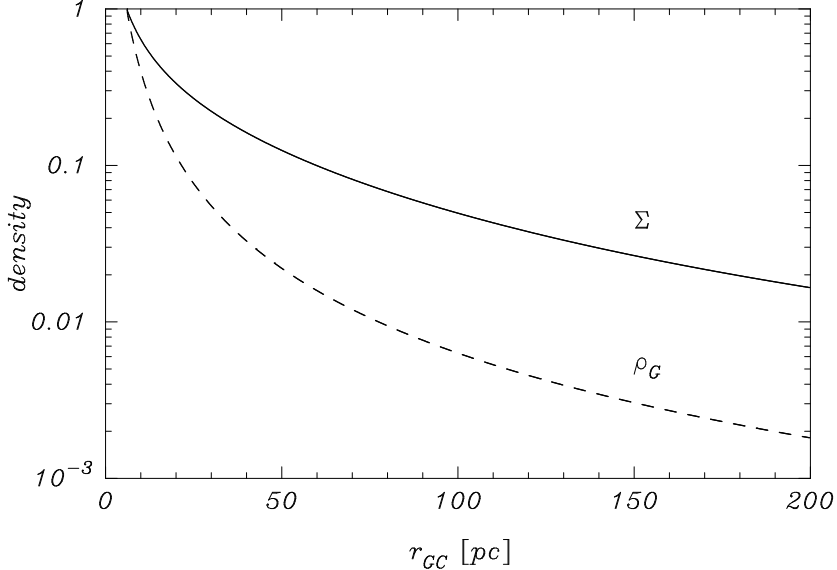


Fig. 11.— Projected (solid line, Eq. 13) and three dimensional (dashed line, Eq. 9) density as a function of the distance to the Galactic center. Both densities are normalized to that of a distance of  $r_{\text{GC}} = 5 \text{ pc}$ ,

Figure 11 shows Eq. 13 and Eq. 9 both normalized to their value at  $r_{\text{GC}} = 5 \text{ pc}$ , which are  $\Sigma(r_{\text{GC}} = 5 \text{ pc}) = 1.65 \times 10^5 \text{ M}_\odot \text{ pc}^{-2}$  and  $\rho_G(r_{\text{GC}} = 5 \text{ pc}) = 1.6 \times 10^4 \text{ M}_\odot \text{ pc}^{-3}$ .

The projected density of model R150W1 remains well below the background, and such a cluster could easily remain unseen throughout its entire lifetime. The two initially more concentrated models, R90W4 and R34W7, have projected densities well above the background, at least initially. The cluster farther from the Galactic center has a lower initial density because it is more extended; after the first few million years, it may be hard to see against the dense stellar background. The observation of the Quintuplet provides an upper limit on the critical contrast below which the cluster cannot be detected. We arbitrarily adopt a minimum contrast of three times the projected background density (i.e.  $10^4 \text{ M}_\odot \text{ pc}^{-2}$ ) as a threshold for distinguishing a star cluster from the background. In that case, the 150 pc cluster would be visible for only about 3 million years ( $\sim 5\%$  of its lifetime). The cluster at 34 pc would be visible for almost 9 million years ( $\sim 70\%$  of its lifetime). Thus, although the cluster farther from the Galactic center lives much longer, its visible lifetime is actually less than that of a cluster at smaller Galactocentric radius.

Although not shown in Fig. 10, the surface density evolution of model R34W1 is also consistent with the densities of the observed clusters. On these grounds we therefore can not exclude the possibility that the Arches and Quintuplet systems lie at Galactocentric distances of 34 pc, but in that case they must have been born with very shallow density profiles (which, however, would contradict our earlier analysis from sect. 5.1).

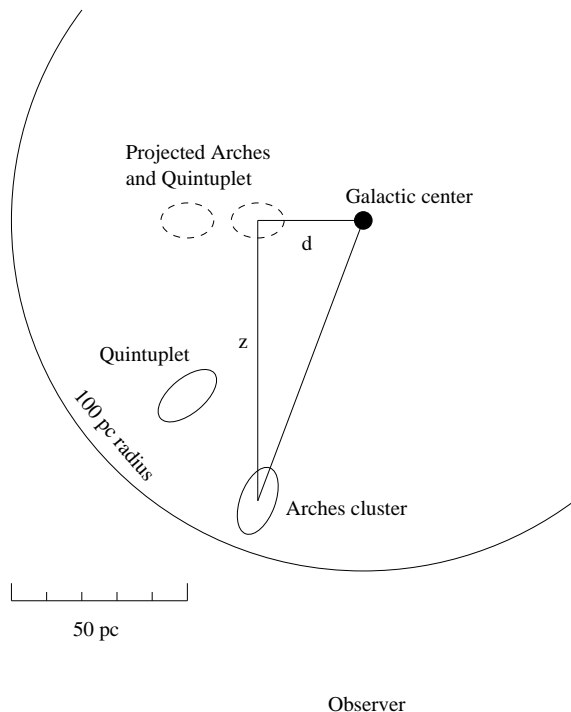


Fig. 12.— Cartoon of the location of the Arches (left) and the Quintuplet (far left) clusters with respect to the Galactic center. Earth is below. The large circle has a radius of 100 pc. The ellipses representing the clusters are exaggerated by a factor of 10.

#### 5.4. The number of hidden clusters near the Galactic center

Although the Arches and Quintuplet clusters are very dense, it may still be difficult to distinguish them near the Galactic center. The three-dimensional density contrast is several orders of magnitude, as can be seen in Fig. 4. In projection on the sky, however, the density contrast is reduced, due mainly to the accumulation of stars along the line of sight. The cluster density within the projected half-mass radius also decreases with time, so these clusters are more easily seen at early ages than at later times. As outlined in the previous subsection, to estimate the time over which our model clusters would be observable, we simply compare the integrated stellar density  $\Sigma(d)$  along the line of sight to the cluster (Eq. 13) with the projected stellar densities of the models.

In the previous subsection we introduced a limiting density contrast above which a cluster can be discriminated from the background stars, and used this to estimate the time during which our models would be detectable. At a Galactocentric distance of 34 pc, our most compact models (R34W7) remain visible for  $\sim 4\text{--}6$  Myr; at 150 pc they become invisible after just 1.5 Myr. Models at greater distances from the Galactic center, or those born with shallower density profiles, remain visible for even shorter times. It is therefore not surprising that the clusters we observe near the Galactic center are extremely compact and very young. Less compact or older clusters are unobservable due to their low surface density contrasts.

Portegies Zwart et al. (2001a) studied the time scale over which clusters such as Arches and the Quintuplet systems remain visible. The results of their detailed N-body calculations are used to calibrate a simple analytical model which is applicable over a wider range of cluster initial conditions. They conclude that clusters within 200 pc of the Galactic center dissolve within  $\sim 70$  Myr. However, their projected densities drop below the background density in the direction of the Galactic center within  $\sim 20$  Myr, effectively making these clusters undetectable after that time. Clusters farther from the Galactic center but at the same projected distance are more strongly affected by this selection effect, and may go undetected for their entire lifetimes. Based on these findings, they conclude that the region within 200 pc of the Galactic center could easily harbor some 50 clusters with properties similar to those of the Arches or the Quintuplet systems. The results of our more extended parameter study is consistent with their findings. Given the higher mass we derive for the Arches cluster (see Tab. 4) compared to what was adopted by Portegies Zwart et al (2001a) we argue that their results are even somewhat conservative and we expect that the region within 200 pc of the Galactic center could easily harbors some 50 clusters with properties similar to those of the Arches or the Quintuplet systems.

Another effect which may contribute to the difficulty in detecting clusters like the Arches is the enormous range in luminosity of the brightest stars. CCD cameras have a dynamic range of less than  $2^{16} = 64\text{k}$ , causing the brightest stars to saturate the detector and preventing faint stars from being detected. However, these brightest stars are also the least common; only with very deep exposures is the rest of the cluster revealed. Thus, wherever two or more bright blue stars are seen together, there may be an entire star cluster lurking in the background.

## 6. Conclusion

We have studied the evolution of young, dense star clusters near the Galactic center, taking the Arches and Quintuplet clusters as specific examples. These clusters are often referred to as “young,” as they are only a few million years old. And indeed, even in a dynamical sense both clusters are quite young, having lifetimes considerably smaller than their initial relaxation times. However, by observing only the most

massive stars in these clusters the dynamical image sketched by the observers is biased toward greater age, as the massive stars evolve dynamically on shorter time scales than average cluster members. By observing only stars with  $m \gtrsim 10 M_{\odot}$ , one selects a part of the cluster that is dynamically rather mature, being comparable in age to the local initial relaxation time. This makes the Arches cluster (and probably also the Quintuplet) appear dynamically older than it really is. We cannot test this hypothesis for the Quintuplet system because the available data are of much lower quality than for the Arches.

The modeled clusters lose mass at a more-or-less constant rate. This rate is inversely proportional to the initial relaxation time, i.e.  $\propto r_{\text{hm}}^{-3/2} \propto r_{\text{GC}}^{-0.9}$  (see also Portegies Zwart et al. 2001a). The star clusters which are born farther away from the Galactic center live therefore considerably longer than those closer in. The relaxation time derived from observation, however, bears little information about the initial relaxation time.

Mass segregation in our model clusters quickly causes the most massive stars to sink into the cluster center. As a result core collapse occurs within two million years, even for models as shallow as  $W_0=1$ . During core collapse close binaries are formed and collisions between stars are frequent. The collision rate is much higher than would be expected from simple cross section arguments, due to mass segregation and binary formation. We confirm the finding of Portegies Zwart et al. (1999) that the most massive stars are generally involved in a collision runaway, in which few low mass stars take part. This process continues until the collision runaway product is ejected by a supernova or a strong encounter with a binary or the cluster dissolves in the tidal field of the Galaxy.

By comparing mass functions from our models at various distances from the cluster center with observations of the Arches mass function, we conclude that the age of the Arches cluster must be about  $0.05 t_{\text{hrx}}$ . With an age of about 1.5 Myr the initial relaxation time of the cluster is then about 30 Myr. To reconcile the observed mass function with the observed density distribution of the Arches, we conclude that the cluster must be about  $4 \times 10^5 M_{\odot}$  and lie some 50 – 90 pc from the Galactic center. With these parameters we can reproduce the observed density distribution and the observed mass function for stars more massive than  $10 M_{\odot}$  without requiring that the initial mass function be different from that found in the solar neighborhood. We therefore conclude that the Arches cluster has a completely “normal” mass function. The observed flat mass function can be explained by selection effects caused by the limited range in distance from the cluster center in which the observations were made.

The young clusters we discussed expand as they become older, causing their surface densities drop. Clusters which are older than about 5 Myr often have surface densities below that of their surrounding, making these clusters virtually undetectable. By comparing the projected density of the model clusters with that of the field stars in the direction of the Galactic center we conclude that the region within 200 pc of the Galactic center could easily harbor some 50 clusters with properties similar to those of the Arches or the Quintuplet systems.

We thank Rob Olling for discussions. This work was supported by NASA through Hubble Fellowship grant HF-01112.01-98A awarded by the Space Telescope Science Institute, which is operated by the Association of Universities for Research in Astronomy, Inc., for NASA under contract NAS 5-26555, by ATP grants NAG5-6964 and NAG5-9264, and by the Research for the Future Program of Japan Society for the Promotion of Science (JSPS-RFTP97P01102). SPZ is grateful to Drexel University, Tokyo University and to the Institute for advanced study for their hospitality and the use of their fabulous hardware. Part of this letter was written while we were visiting the American Museum of Natural History. We acknowledge

the hospitality of their astrophysics department and visualization group. We thank the Alfred P. Sloan Foundation for a grant to Hut for observing astrophysical computer simulations in the Hayden Planetarium at the Museum.

## REFERENCES

Bahcall, J. N., Soneira, R. M. 1980, *ApJS*, 44, 73

Baumgardt, H. 2000, in *MNRAS* in press, 10 pages, 13 figures., 12330

Blum, R. D., Damineli, A., Conti, P. S. 1999, *AJ*, 117, 1392

Brandl, B., Brandner, W., Eisenhauer, F., Moffat, A. F. J., Palla, F., Zinnecker, H. 1999, *A&A*, 352, L69

Brandl, B., Sams, B. J., Bertoldi, F., Eckart, A., Genzel, R., Drapatz, S., Hofmann, R., Loewe, M., Quirrenbach, A. 1996, *ApJ*, 466, 254

Campbell, B., Hunter, D. A., Holtzman, J. A., Lauer, T. R., Shayer, E. J., Code, A., Faber, S. M., Groth, E. J., Light, R. M., Lynds, R., O'Neil, E. J., J., Westphal, J. A. 1992, *AJ*, 104, 1721

Figuer, D. F., Kim, S. S., Morris, M., Serabyn, E., Rich, R. M., McLean, I. S. 1999a, *ApJ*, 525, 750

Figuer, D. F., McLean, I. S., Morris, M. 1999b, *ApJ*, 514, 202

Giersz, M., Heggie, D. C. 1994, *MNRAS*, 268, 257

Giersz, M., Heggie, D. C. 1996, *MNRAS*, 279, 1037

Glass, I. S., Catchpole, R. M., Whitelock, P. A. 1987, *MNRAS*, 227, 373

Heggie, D. C., Mathieu, R. 1986, *MNRAS*, in P. Hut, S. McMillan (eds.), *Lecture Not. Phys* 267, Springer-Verlag, Berlin

Heggie, D. C., Ramamani, N. 1995, *MNRAS*, 272, 317

Hill, G., Hilditch, R. W., Barnes, J. V. 1979, *MNRAS*, 186, 813

King, I. R. 1966, *AJ*, 71, 64

Kippenhahn, R., Weigert, A. 1967, *Zeitschr. f. Astroph.*, 65, 251

Makino, J. 1991, *ApJ*, 369, 200

Makino, J., Aarseth, S. J. 1992, *PASJ*, 44, 141

Makino, J., Taiji, M., Ebisuzaki, T., Sugimoto, D. 1997, *ApJ*, 480, 432

Massey, P., Hunter, D. A. 1998, *ApJ*, 493, 180

McMillan, S. L. W. 1986a, *ApJ*, 306, 552

McMillan, S. L. W. 1986b, *ApJ*, 307, 126

Mezger, P. G., Zylka, R., Philipp, S., Launhardt, R. 1999, *A&A*, 348, 457

Nagata, T., Woodward, C. E., Shure, M., Kobayashi, N. 1995, AJ, 109, 1676

Nagata, T., Woodward, C. E., Shure, M., Pipher, J. L., Okuda, H. 1990, ApJ, 351, 83

Okuda, H., Shibai, H., Nakagawa, T., Matsuhara, H., Kobayashi, Y., Kaifu, N., Nagata, T., Gatley, I., Geballe, T. R. 1990, ApJ, 351, 89

Olling, R. P., Merrifield, M. R. 1998, MNRAS, 297, 943

Oort, J. 1927, *ban*, 3, 275

Portegies Zwart, S. F., Hut, P., Makino, J., McMillan, S. L. W. 1998, A&A, 337, 363

Portegies Zwart, S. F., Hut, P., Verbunt, F. 1997, A&A, 328, 130

Portegies Zwart, S. F., Makino, J., McMillan, S. L. W., Hut, P. 1999, A&A, 348, 117

Portegies Zwart, S. F., Makino, J., McMillan, S. L. W., Hut, P. 2001a, ApJ, 546, L101

Portegies Zwart, S. F., McMillan, S. L. W., Hut, P., Makino, J. 2001b, MNRAS, 321, 199

Portegies Zwart, S. F., Verbunt, F. 1996, A&A, 309, 179

Scalo, J. M. 1986, Fund. of Cosm. Phys., 11, 1

Serabyn, E., Shupe, D., Figer, D. F. 1998, Nature, 394, 448

Spitzer, L. 1987, *Dynamical evolution of globular clusters*, Princeton, NJ, Princeton University Press, 1987, 191 p.

Takahashi, K., Portegies Zwart, S. F. 2000, ApJ, 535, 759

Vesperini, E., Heggie, D. C. 1997, MNRAS, 289, 898

Vrba, F. J., Henden, A. A., Luginbuhl, C. B., Guetter, H. H., Hartmann, D. H., Klose, S. 2000, ApJ, 533, L17